

Investigating the doping effects on the optical, electrical, structural, morphological, elemental composition, and magnetic properties of electrodeposited Ti-doped CuS thin films

Emmanuel O. Okechukwu,^{1*} Azubuikwe J. Ekpunobi,¹ A.C.O. Azubogu,² E.N. Onuigbo,³ Overcomer Anusiuba,⁴ Adline Nwodo,⁵ Diemiruaye M. Jeroh,¹ Chukwudi B. Muomeliri,¹ Chidozie E. Okafor,¹ Lynda Ozobialu,¹ Chiamaka P. Onu,¹ Uche E. Ekpunobi,⁶ Nonso L. Okoli,⁷ E.U. Ogbodo^{2,8}

¹Department of Physics and Industrial Physics, Nnamdi Azikiwe University, Awka, Nigeria. ²Department of Electronics and Computer Engineering, Nnamdi Azikiwe University, Awka, Nigeria. ³Department of Geological Sciences, Nnamdi Azikiwe University, Awka, Nigeria. ⁴Department of Computer Science, Nnamdi Azikiwe University, Awka, Nigeria. ⁵Magnetism and Magnetoscience Laboratory, Kagoshima University, Japan. ⁶Department of Pure and Industrial Chemistry, Nnamdi Azikiwe University, Awka, Nigeria. ⁷Nanoscience and Advanced Materials, Federal University of ABC, Santo Andre, Sao Paulo, Brazil. ⁸Department of Electrical Engineering, Tshwane University of Technology, South Africa.

Submitted on: 21-Mar-2025, Revised: 20-Jun-2025, Accepted on: 20-Jun-2025, Published on: 21-Jun-2025

Article

ABSTRACT

Thin films of copper(II) sulfide (CuS) and titanium-doped copper(II) sulfide (Ti:CuS) were successfully deposited on fluorine-doped tin oxide (FTO) glass substrates using the electrodeposition technique at room temperature. The films were characterized to evaluate their optical, structural, morphological, compositional, electrical, and magnetic properties. The

characterization techniques included UV-Vis spectrophotometry (in the wavelength range of 300–1100 nm), X-ray diffraction (XRD), scanning electron microscopy (SEM) equipped with energy-dispersive X-ray spectroscopy (EDX), four-point probe method, and vibrating sample magnetometry (VSM). Film thicknesses were measured using a profilometer, yielding values of 109.16 nm for undoped CuS, and 121.11 nm, and 131.79 nm for 2%, 6%, and 10% Ti-doped CuS thin films, respectively. The optical bandgap of the films ranged between 2.40 eV and 2.60 eV. Structural analysis confirmed the hexagonal phase of CuS, with lattice constants $a = b = 3.7920 \text{ \AA}$ and $c = 16.3440 \text{ \AA}$.

Keywords: electrodeposition, Ti doping, bandgap, UV-VIS spectroscopy, XRD, SEM-EDS, four-point probe

INTRODUCTION

In the pursuit of materials with unique properties for advanced technological applications, the synthesis and characterization of dilute magnetic semiconductor (DMS) films have attracted significant research interest in recent years. Among the most recently studied are thin films of copper(II) sulfide doped with

titanium ions, owing to their distinctive spintronic properties. Dilute magnetic semiconductors (DMSs) are materials that exhibit both semiconducting and magnetic properties [1]. They are typically produced by incorporating a small amount of magnetic elements, such as transition metals, into the crystal lattice of a semiconductor. This doping process maintains the original lattice structure while imparting magnetic characteristics, making DMSs suitable for a wide range of modern electronic and spintronic devices. [2]. The doping introduces a localized magnetic moment that can interact with the electron spin in the semiconductor. Dilute magnetic semiconductors have their promising applications in spintronics

*Corresponding Author: Emmanuel O. Okechukwu, Email: emmynuelsy@yahoo.com



[3-5], where electron spin is utilized for information storage and processing [6], quantum bits for quantum computation and communication [7], nanoscale integrated magnetic memories and sensors [8], data storage [9], magneto-optoelectronic devices [10].

Among different metal chalcogenides, copper sulfide has been extensively studied and has attracted much interest in the recent research due to its special properties and potential applications such as in solar cells [11], cathode material in lithium chargeable batteries [12], optical data storage [13], fabrication of microelectronic devices, optical filters as well as in low temperature gas sensor applications [14], gas sensors [15], photochemical conversion of solar energy as solar absorber coating and photoconductive coatings [16].

Thin films of copper sulfide have been grown using various techniques, which include chemical bath deposition (CBD) [17], chemical spray pyrolysis (CSP) [18, 19], atomic layer deposition (ALD) [20], electrodeposition [21], and pulsed laser deposition (PLD) technique [22]. Among them all, electrodeposition has been considered the best deposition technique, because of its advantages such as: low cost effective, simplicity, high growth rate at relatively low temperature, and easier control of film thickness, morphology, and composition [23-26].

Our present work gears towards doping copper (II) sulfide (CuS) thin films with titanium (Ti) impurities, so as to investigate their unique properties, for possible technological applications, using the simple and low-cost electrodeposition technique.

2. EXPERIMENTAL PROCEDURE

Materials and Method

Three-electrode cell set-up was adopted in the films' deposition, where we used the FTO as the working electrode, silver – silver chloride electrode (Ag/AgCl) as reference electrode, and platinum wire as a counter electrode. The glass substrates were ultrasonically cleaned in ethanol for 30 minutes (at 30 °C), rinsed with distilled water, and allowed to dry before use.

2.1 Deposition Of Undoped Copper (II) Sulphide (CuS) Thin Film

The bath solution for the deposition of CuS thin films contained 15 ml of 0.05 molar concentration of copper (ii) sulphate pentahydrate (CuSO₄.5H₂O) as a source of copper ion (Cu²⁺) and 15 ml of 0.05 molar concentration of thiourea (CH₄N₂S) as a source of sulfur ion (S²⁻). The solution was mixed properly using a magnetic stirrer. The 0.05 M of CuSO₄.5H₂O was prepared by dissolving 6.2 g of it in 500 ml of distilled water; and the 0.05 M of CH₄N₂S was prepared by dissolving 1.9 g of it 500 ml of distilled water. The film deposition took place at room temperature of 27 °C. The pH value (2.9) of the bath solution was obtained using a pH meter. The deposition time and voltage were kept at 10 s and 5 V respectively, as shown in Table 1. After deposition, the sample was taken out of the solution carefully, and immersed in distilled water for just two seconds, and then allowed to dry in flowing air. Afterwards, the sample was placed in a slide box, labelled accordingly.

Table 1: Deposition of CuS thin film

Sam ple	CuSO ₄ .5H ₂ O		CH ₄ N ₂ S		pH	Te mpe ratur e (°C)	Volt age (V)	Ti me (s)
	Conc. (M)	Vol. (ml)	Conc. (M)	Vol. (ml)				
CuS	0.05	15	0.05	15	2.5	27	5	10

2.2 Deposition Of Ti-doped Copper (II) Sulphide (Ti :CuS) Thin Films

The combination of ionic concentrations for doping of CuS with titanium is given in Table 2. By varying the relative ratio of Cu and Ti ions, the Cu_{1-x}Ti_xS films with solution parameter x = 0.00, 0.02, 0.06, and 0.10 were deposited. The percentage doping was varied from 2% - 10% at an interval of 4%.

Table 2: Doping formulations of precursors used for deposition of Cu_{1-x}Ti_xS

Composit ion parameter (x)	Percenta ge doping (%)	Concentrati on of copper sulphate (mole)	Concentrati on of titanium chloride (mole)	Concentrati on of thiourea (mole)
0.00	0	0.050	0.000	0.050
0.02	2	0.049	0.001	0.050
0.06	6	0.047	0.003	0.050
0.10	10	0.045	0.005	0.050

During deposition, pH of the solution bath was kept at a constant value of 2.2, using ammonia solution (NH₃), and the films' deposition took place at room temperature of 27 °C, voltage value of 5 V, and time of 10 s, as given in Table 3.

Table 3: Variation of percentage doping for the deposition of Cu_{1-x}Ti_xS Thin Films

Sam ple	CuSO ₄ .5H ₂ O Co nc.(M)	Vo l.(ml)	TiCl ₃ Co nc.(M)	Vo l.(ml)	CH ₄ N ₂ S Co nc.(M)	Vo l.(ml)	NH ₃ Co nc.(M)	p H	Te m p e r a t u r e (° C)	Do p i ng (%)	Vo l t a g e (V)	T i m e (s)
Cu S	0.0 50	15	0.0 00	10	0.0 50	15	0.0 5	2	27	5	10	
Ti: 2%	0.0 49	15	0.0 01	10	0.0 50	15	0.0 50	2	27	6	10	
Ti: 6%	0.0 47	15	0.0 03	10	0.0 50	15	0.0 50	2	27	10	10	
Ti: 10 %	0.0 45	15	0.0 05	10	0.0 50	15	0.0 50	2	27	10	10	

3 Film Characterization

The deposited films were characterized in order to investigate their optical, electrical, structural, morphological, compositional, and magnetic properties. The optical characterization was done using a UV-VIS spectrophotometer (model: 756S UV-VIS) to obtain the optical absorption data of the films, within the wavelength range of 300 nm - 1100 nm. Four-point probe technique (Keithley 2400 – LV source meter) was employed to analyse the electrical properties of the films. The films structural properties were studied using an X-ray diffractometer (Bruker D8 high-resolution diffractometer) using Cu K α line ($\lambda = 1.54056 \text{ \AA}$). Surface morphology and elemental composition of the films

were also studied using Nova NanoSEM and MIRA TESCAN SEM machine. The magnetic properties of the films were obtained using vibrating sample magnetometer (Model: EZ 10 by MicroSense), while the films thicknesses were measured with the aid of a profilometer (Model: Veeco Dektak 150).

RESULTS AND DISCUSSION

4.1 Effect of titanium concentration on the thickness of CuS thin films

Figure 4.1 depicts the effect of titanium concentration on the thickness of CuS thin films.

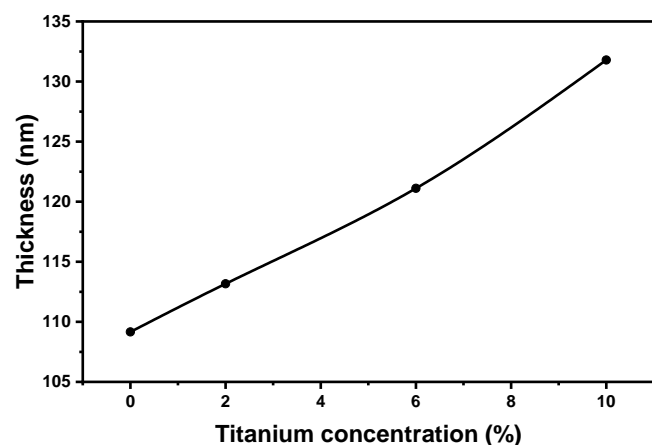


Figure 4.1: Effect of titanium concentration on the thickness of CuS thin films

The figure revealed a linear increase in the thickness of the films (from 109.16 nm to 131.79 nm) as titanium concentration was increased from 2 % to 10%.

4.2 Optical Analysis

From the measured absorbance data of the undoped and titanium-doped copper (II) sulfide thin films, the optical properties of the films, such as the transmittance (T), the reflectance (R), the refractive index, extinction coefficient, optical conductivity, energy band gap, real and imaginary dielectric constants, were evaluated using the appropriate equations. The transmittance (T) of the deposited films was evaluated using $T = 10^{-A}$ [28, 29], where A is the absorbance. While $R = 1 - (A + T)$ as given by [30, 31], was used to evaluate the reflectance (R) of the deposited films.

4.2.1 Absorbance (A), Transmittance (T), and Reflectance (R) Plots

Plots of the absorbance, transmittance, and reflectance of the deposited films of undoped copper (II) sulfide (CuS) and titanium-doped copper (II) sulfide (Ti:CuS) are depicted in Figure 4 (a-c).

The optical absorption coefficient (α) of the films was calculated using equation (5), as given by [32-34]:

$$\alpha = \frac{1}{t} \ln \left(\frac{1}{T} \right) \quad (5)$$

Where t is the thickness of the films and T is the transmittance. The extinction coefficient (K) of the deposited films was evaluated using equation (6), as given by [35, 36]:

$$k = \frac{\alpha \lambda}{4\pi} \quad (6)$$

The refractive indices of the samples were calculated using equation (7), as given by [37, 38]:

$$\eta = \frac{1+R}{1-R} + \sqrt{\frac{4R}{(1-R)^2} - k^2} \quad (7)$$

The optical conductivity (σ_o) of the films was calculated using equation (8), as given by [39, 40]:

$$\sigma_o = \frac{\alpha \eta c}{4\pi} \quad (8)$$

where c is the speed of light. The energy band gap of the films was calculated using Tauc's formula for near-band edge absorption, as given by [41 - 44]:

$$(\alpha h\nu)^n = A(h\nu - E_g) \quad (9)$$

where α is the optical absorption coefficient, A is the transition probability constant, h is the Planck's constant, ν is the frequency of incident radiation, E_g is the band gap of the films and n is the characteristic constant for the optical transition. The optical band gap energy (E_g) of our deposited films were obtained by extrapolating the straight portion of the plot of $(\alpha h\nu)^2$ against the photon energy ($h\nu$) at $(\alpha h\nu)^2 = 0$. The films' complex dielectric function was estimated from the relation given by [45, 46]:

$$\epsilon = \epsilon_r + i\epsilon_i \quad (10)$$

$$\epsilon_r = n^2 - k^2 \quad (11)$$

$$\epsilon_i = 2nk \quad (12)$$

Where ϵ_r and ϵ_i are the real and imaginary parts of the dielectric constant, respectively. Figures (4.2), (4.3), and (4.4) show the absorption spectral, transmittance, and reflectance of the undoped CuS and Ti-doped CuS thin films, respectively.

From Figure 4.2, the absorbance spectra showed a uniform decrease in absorbance as photon wavelength increased across UV and VIS regions, with a very slight increase within the NIR region. Also, absorbance was found to have increased as percentage of titanium increased. The increase in absorption of photon energy is evidence that there is substitution of copper ions by titanium ions in the lattice structure of copper sulfide. Figure 4.3 revealed that the transmittance values of the films increased uniformly with increase in wavelength within UV and VIS regions, but showed a slight decrease at NIR region. This high transmission indicates the high level of homogeneity of the films. Also, transmission of the films was found to decrease as the dopant concentration was increased. Reflectance of the thin films increased within UV region, as wavelength increased, with the exception of the undoped and 2 % Ti doped copper sulfide thin films that started decreasing from the UV region, as shown in Figure 4.4. From the results obtained, Ti-doped CuS films recorded low reflection compared to the undoped CuS films. This could be attributed to the high absorbance nature of the films, caused by the thickness, which increased as the titanium percentage concentration was increased. The results showed that these films are good absorber of photon energy within the visible region and could be used to shed UV radiation and for antireflective coatings.

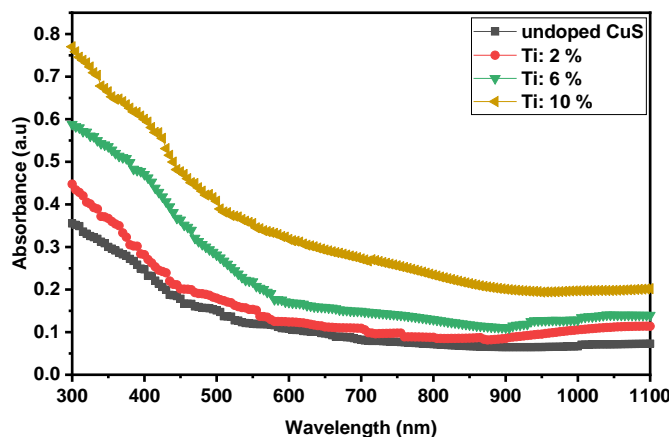


Figure 4.2: Plot of absorbance against wavelength for undoped and titanium-doped copper (II) sulfide thin films deposited at different titanium concentrations.

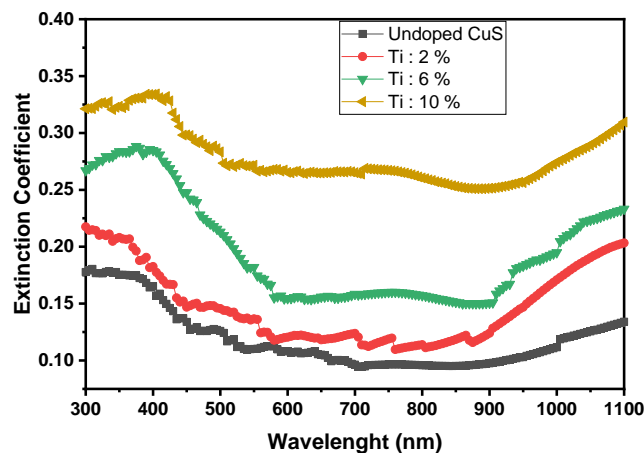


Figure 4.5: Plot of extinction coefficient against wavelength for undoped and titanium-doped copper (II) sulfide thin films deposited at different titanium concentrations.

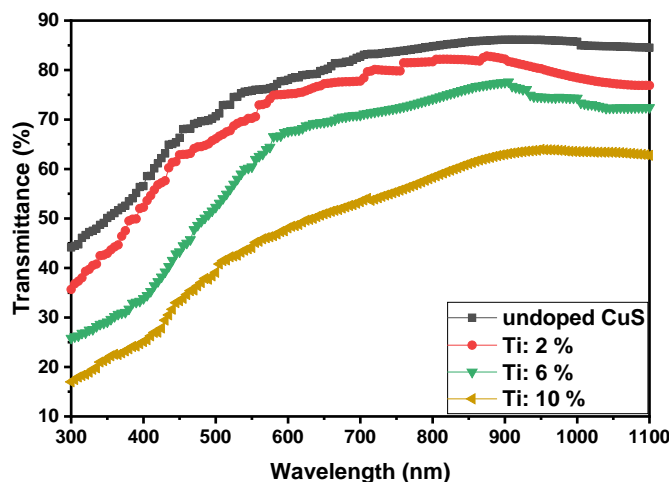


Figure 4.3: Plot of transmittance against wavelength for undoped and titanium-doped copper (II) sulfide thin films deposited at different titanium concentrations

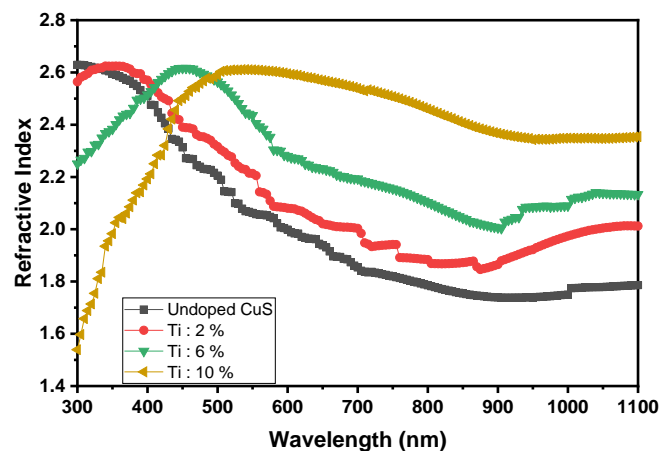


Figure 4.6: Plot of refractive index against wavelength for undoped and titanium-doped copper sulfide (II) thin films deposited at different titanium concentrations

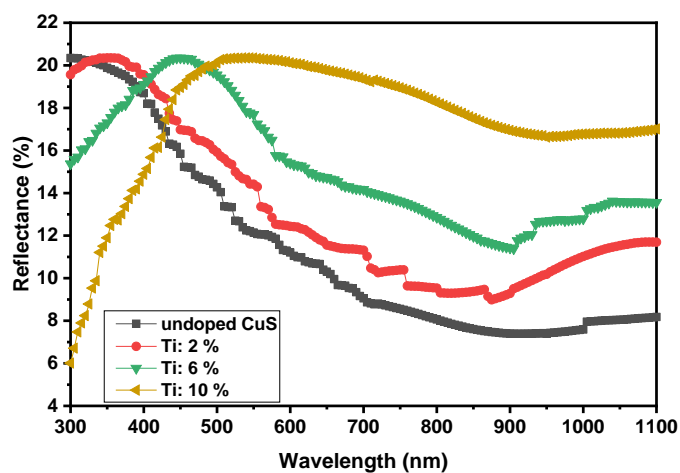


Figure 4.4: Plot of reflectance against wavelength for undoped and titanium-doped copper (II) sulfide thin films deposited at different titanium concentrations.

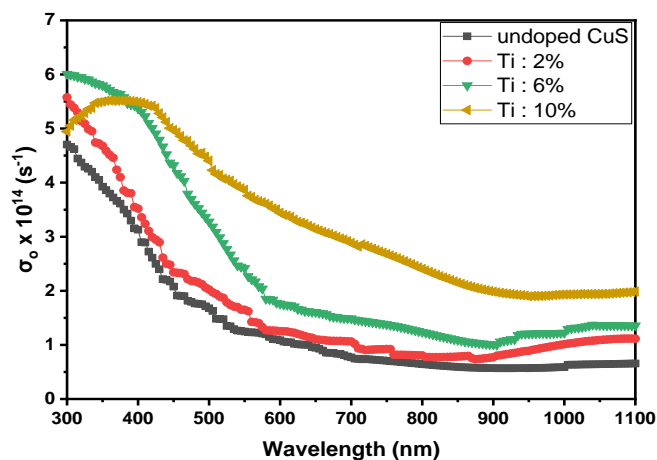


Figure 4.7: Plot of optical conductivity against wavelength for undoped and titanium-doped copper (II) sulfide thin films deposited at different titanium concentrations.

Figures 4.5 – 4.9 show the plots of extinction coefficient, refractive index, optical conductivity, real, and imaginary dielectric constants of the films, respectively.

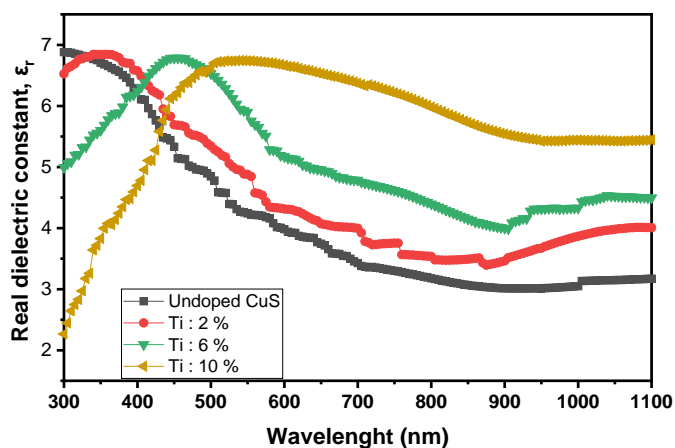


Figure 4.8: Plot of real dielectric constant against wavelength for undoped and titanium-doped copper (II) sulfide thin films deposited at different titanium concentrations.

The graph (Fig. 4.5) revealed that the extinction coefficient of undoped CuS films decreased within UV-VIS (300 nm – 700 nm) regions, and increased at NIR region (800 nm), while Ti-doped CuS films decreased as wavelength increased from 300 nm – 560 nm, then remained steady before increasing at 880 nm. From Fig. 4.6, the result obtained showed that refractive index of the films was reducing (at 300 nm), as doping percentage concentration was increased. The result shown in Fig. 4.7 is a revelation of the fact that, as Ti doping concentration was increased from 2 % to 6 %, the optical conductivity values increased, and then decreased beyond 6 % doping concentration (at 300 nm). Also, the Figure showed that optical conductivity of the deposited thin films decreased with increased wavelength. From Fig. 4.8, it can be observed that the undoped CuS thin film recorded the highest real dielectric constant within UV region. But with the introduction of titanium ion as a doping agent, the real dielectric constant decreased within the UV region. Furthermore, within the VIS region, real dielectric constant increased with doping concentration. The graph (Fig. 4.9) showed that the imaginary dielectric constant of the films decreased (from 350 nm) within UV – VIS region, but increased within NIR region. Also, the results obtained across the

wavelengths showed that imaginary dielectric constant values increased with the doping concentration.

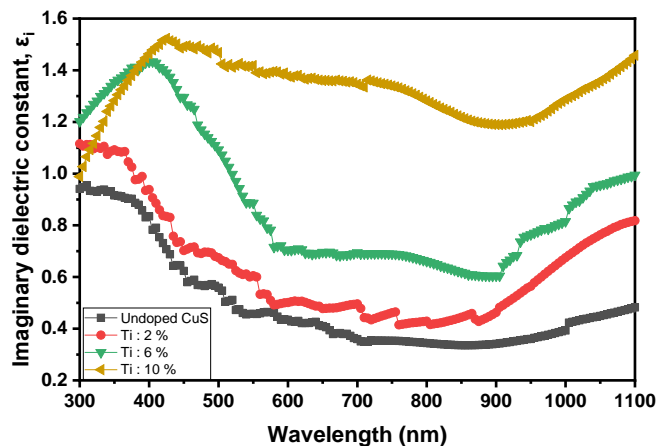


Figure 4.9: Plot of imaginary dielectric constant against wavelength for undoped and titanium-doped copper (II) sulfide thin films deposited at different titanium concentrations.

Figure 4.10 is the plot of $(\alpha h\nu)^2$ against photon energy for undoped and titanium-doped copper (II) sulfide thin films. From the graph, energy band gap of the films were estimated by extrapolation of the straight portion of the graph along the photon

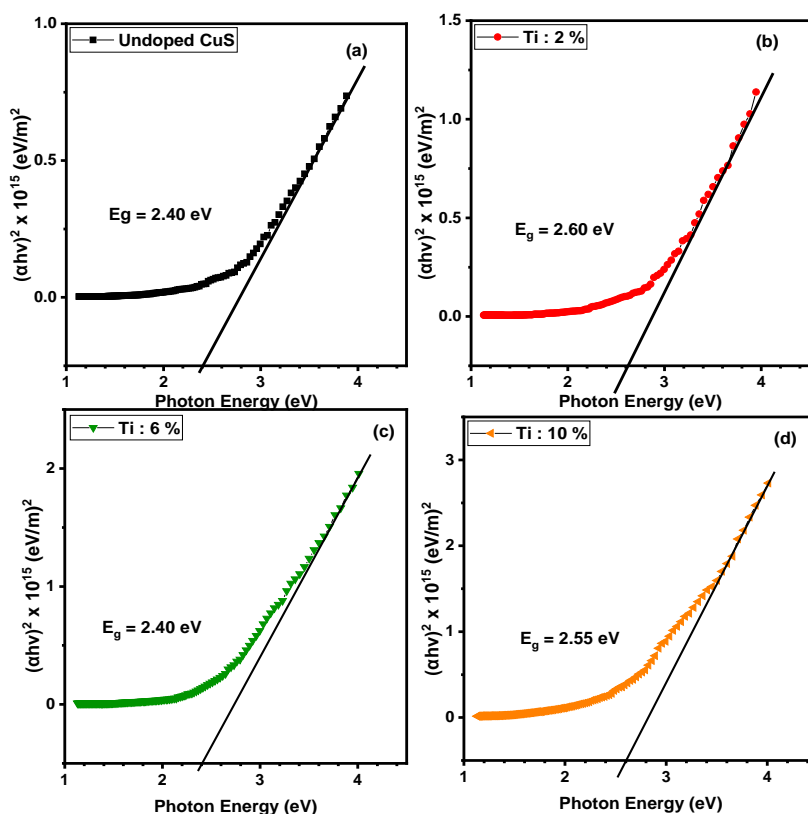


Figure 4.10: Plot of $(\alpha h\nu)^2$ against photon energy for undoped and titanium-doped copper (II) sulfide thin films deposited at different titanium concentrations

energy axis where $(ahv)^2 = 0$. Energy band gap of 2.40 eV, 2.60 eV, 2.40 eV, and 2.55 eV, were recorded for the undoped CuS thin film, 2 %, 6 %, and 10 % titanium-doped CuS thin films, respectively. As it is shown in the figure, the introduction of titanium dopant (2 %) into the precursor of copper sulfide thin film, altered the energy bandgap of the deposited CuS film. This is based on the fact stated by [47], that titanium doping can increase the carrier concentrations and shift the Fermi level towards the conduction band that leads to shift in absorption edge towards the higher energies. However, at 6 % doping, the energy bandgap dropped to a value similar to the undoped CuS film (2.40 eV), which could be as a result of the possibility of formation of some related titanium phases such as TiS, with the same energy bandgap as the undoped CuS film. The energy bandgap increased further with higher percentage doping (10 %).

4.3 Structural Analysis

Fig. 4.11 reveals the XRD pattern of the films, which was used to analyze the structural behavior of the electrodeposited films.

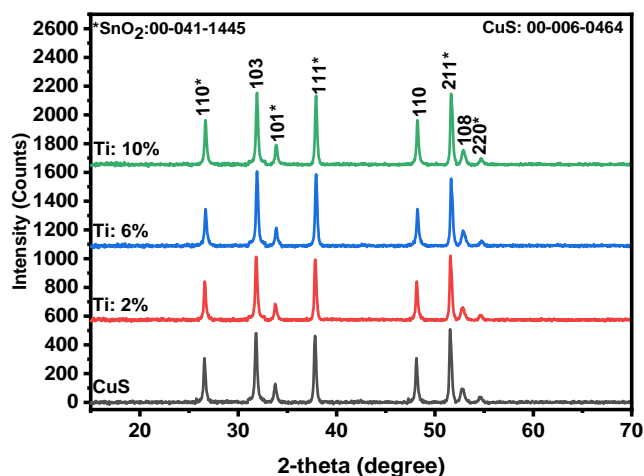


Figure 4.11 (a): Structural patterns of undoped and Ti-doped copper (II) sulfide thin films

The matching of the calculated d_{hkl} values and the standard ones confirms that all the deposited films crystallize well in the hexagonal structure with preferential orientation of the crystallites along the (103) direction with 2 theta angles of 31.813 °, 31.841 °, 31.919 °, and 31.910 ° for the undoped and titanium-doped copper sulfide thin films, respectively, and lattice constant $a=b= 3.7920 \text{ \AA}$ and $c = 16.3440 \text{ \AA}$. Increase in dopant concentration caused an increase in intensity of the diffraction peaks and shift in the peaks towards larger angles as can be observed in Table 4.7. Peak shift towards higher angles as titanium ion concentration was increased could be due to the fact that titanium ions simply occupied copper ions' sites. This substitutional occupation of copper ion sites by titanium ions, caused peak shift towards higher angles due to expansion of the lattice constant of the host ion (Cu^{2+}). The average crystal sizes (range from 27.761 nm to 31.455 nm) shown in Table 4.3 were calculated using Debye-Scherrer's relation [48, 49] given as:

$$D = \frac{k\lambda}{\beta \cos \theta} \quad (13)$$

Where $k = 0.9$ (the shape factor); $\lambda = \text{X-ray wavelength}$; $\beta = \text{Full Width Half Maximum}$; and $D = \text{grain size}$.

From the values of the crystallite size obtained, the dislocation density (δ), the microstrain (ϵ) and the inter-planer spacing (d) [50] of the deposited films, were calculated using equations (14), (15) and (16), respectively:

$$\delta = \frac{1}{D^2} \quad (14)$$

$$\epsilon = \frac{\beta}{4 \tan \theta} \quad (15)$$

$$d = \frac{\lambda}{2 \sin \theta} \quad (16)$$

The XRD results obtained showed that, with the increase in dopant percentage, crystallite size of the films increased, while dislocation density and micro-strain decreased. This could be attributed to improvement in the crystal structure due to titanium ion doping. Figure 4.11 (b) shows the variation of crystallite size and dislocation density with concentration of dopant ion (titanium ion).

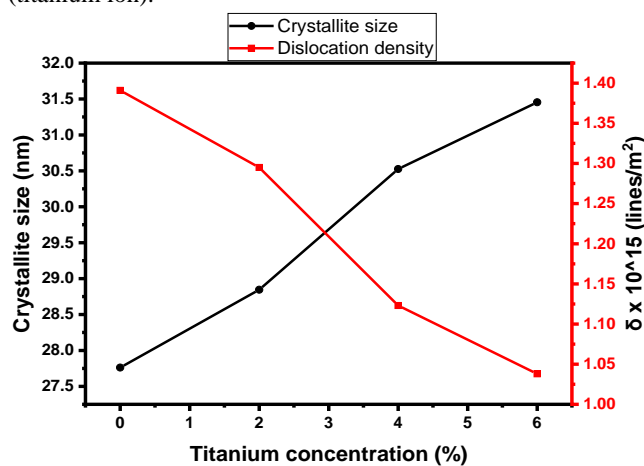


Figure 4.11 (b): Variation of crystallite size and dislocation density with titanium ion concentration for undoped and titanium-doped copper sulfide (II) thin films

Table 4.3: Structural parameters of Ti-doped copper (II) sulfide thin films at varied concentrations of titanium ions

Sample s	2 θ (°)	hkl	d - spacinq (nm)	FWHM M (°)	D (nm)	$\delta \times 10^{15}$ (lines/m ²)	$\epsilon \times 10^{-3}$
CuS	26.58	110			29.44		5.34
	3	*	3.351	0.290	8	1.153	8
	31.81	103			28.46		4.64
	3		2.811	0.303	8	1.234	0
	33.76	101			25.99		4.79
	8	*	2.652	0.334	2	1.480	6
	37.81	111			31.38		3.56
	6	*	2.377	0.279	1	1.015	0
	48.13	110			31.38		2.82
	0		1.889	0.290	4	1.015	9
	51.58	211			30.74		2.70
	2	*	1.770	0.300	3	1.058	7

	52.79	108			19.75	4.12
	7		1.733	0.469	0	2.564
	54.62	220			24.91	3.16
	7	*	1.679	0.375	9	1.610
	Average				27.76	1.391
					1	6
Ti: 2%	26.61	110			31.21	5.03
	3	*	3.347	0.273	7	1.026
	31.84	103			28.98	4.55
	1		2.808	0.298	5	1.190
	33.79	101			26.86	4.63
	8	*	2.650	0.323	9	1.385
	37.84	111			32.18	3.46
	5	*	2.375	0.273	9	0.965
	48.16	110			33.27	2.66
	0		1.888	0.273	3	0.903
	51.61	211			31.54	2.63
	2	*	1.769	0.292	4	1.005
	52.82	108			20.11	4.04
	3		1.732	0.461	1	2.472
	54.65	220			26.57	2.96
	2	*	1.678	0.351	9	1.416
	Average				28.84	1.295
					6	2
Ti: 6%	26.69	110			34.16	4.59
	1	*	3.337	0.250	0	0.857
	31.91	103			29.14	4.51
	9		2.802	0.296	1	1.178
	33.87	101			26.52	4.68
	1	*	2.644	0.327	5	1.421
	37.92	111			31.90	3.49
	3	*	2.371	0.275	7	0.982
	48.23	110			32.51	2.72
	8		1.885	0.280	3	0.946
	51.68	211			36.82	2.25
	3	*	1.767	0.250	3	0.738
	52.90	108			24.99	3.25
	1		1.729	0.371	8	1.600
	54.73	220			28.13	2.79
	7	*	1.676	0.332	7	1.263
	Average				30.52	1.123
					5	0
Ti: 10%	26.68	110			29.98	5.23
	4	*	3.338	0.284	9	1.112
	31.91	103			29.87	4.40
	0		2.802	0.289	1	1.121
	33.87	101			32.08	3.87
	2	*	2.644	0.270	9	0.971
	37.91	111			32.85	3.39
	4	*	2.371	0.267	7	0.926
	48.23	110			31.97	2.77
	1		1.885	0.284	3	0.978
	51.68	211			38.57	2.15
	3	*	1.767	0.239	6	0.672
	52.90	108			27.79	2.92
	2		1.729	0.333	7	1.294
	54.71	220			28.48	2.76
	6	*	1.676	0.328	4	1.233
	Average				31.45	1.038
					5	0

4.4 SEM analyses

Figure 4.12 shows the SEM images of undoped and titanium-doped copper (II) sulfide thin films deposited at different concentration of titanium ions. The SEM images revealed agglomerated particles of different sizes and shapes. The undoped copper (II) sulfide film contained spherical-like particle sizes that are less densely packed. The surface morphology of the film deposited at titanium concentration of 2 % showed the formation of larger spherical-like particles that are not well distributed on the substrate when compared to the undoped copper (II) sulfide film. Increasing the doping concentration to 6 % leads to the increase in the number of clusters and agglomerated nanoparticles. At further increase in doping concentration (10 %), the particle sizes of the film decreased, and the grains became unevenly distributed on the substrate. From the results, however, particles of the films are of unequal distribution, which suggest formation of polycrystalline thin films of copper sulfide and titanium-doped copper (II) sulfide thin films.

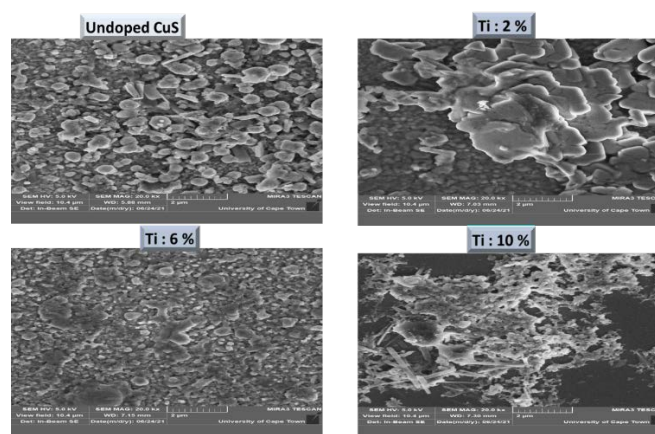


Figure 4.12: SEM images of undoped and titanium-doped copper (II) sulfide thin films at different percentages of titanium ion

4.5 EDS analyses

Figure 4.13 (a) and (b) showcase the elemental composition of the undoped copper (II) sulfide and titanium-doped copper sulfide thin films, respectively. Fig. 4.13 (a) confirms the presence of the anticipated elements (Cu and S) in the deposited film, but with some impurity atoms. Also, Fig. 4.13 (b) confirms the presence of the anticipated elements (Cu, S, and Ti) in the deposited film, but with some impurity atoms. The presence of impurity atoms (silicon, calcium, and oxygen), was as a result of the composition of the glass substrate.

4.6 Electrical Analyses

Electrical properties of titanium-doped copper (II) sulfide thin films synthesized at different titanium ion concentration are shown in Table 4.4. The result revealed a variation in the electrical properties due to the doping of copper (II) sulfide with titanium ion. Electrical resistivity value of $58.89 \times 10^{-5} \Omega m$ and conductivity of $1.70 \times 10^3 (S/m)$ were obtained for the undoped CuS thin film. Close observation showed that immediately titanium ion was introduced, the films' resistivity value decreased to $11.37 \times 10^{-5} (\Omega m)$, and decreased further to

$7.68 \times 10^{-5} \Omega m$, as percentage doping was increased from 2 % to 6 %. But at peak value of 10 %, the resistivity value slightly increased to $9.34 \times 10^{-5} \Omega m$. While the films' resistivity was decreasing, the electrical conductivity of the films was found to have increased from $8.70 \times 10^3 S/m$ to $13.02 \times 10^3 S/m$, which later decreased to $10.71 \times 10^3 S/m$ as the resistivity value increased [61]. The decrease in electrical conductivity could be attributed to the increase in the thickness of the deposited thin films, due to the increase in titanium ion concentration. The graph of electrical resistivity and conductivity against percentage of titanium ion is shown in Figure 4.14.

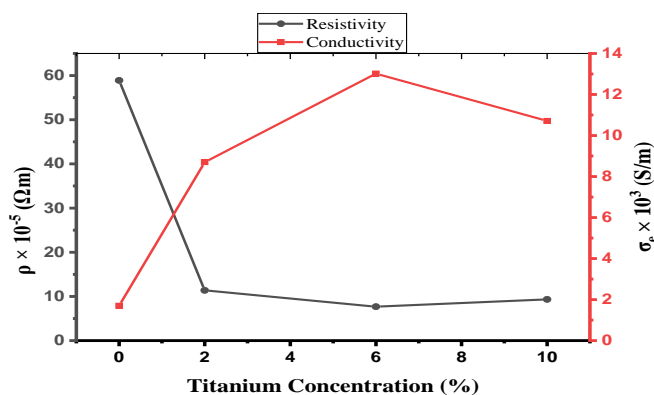


Figure 4.14: Variation of electrical resistivity and conductivity with percentage of titanium ion.

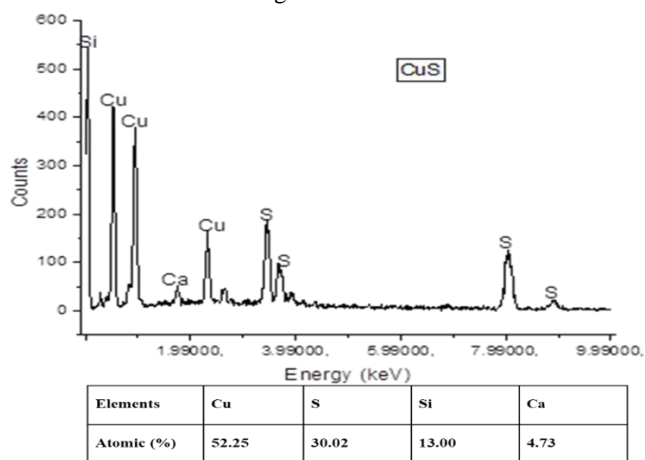


Figure 4.13 (a): EDS graph of the undoped CuS thin film

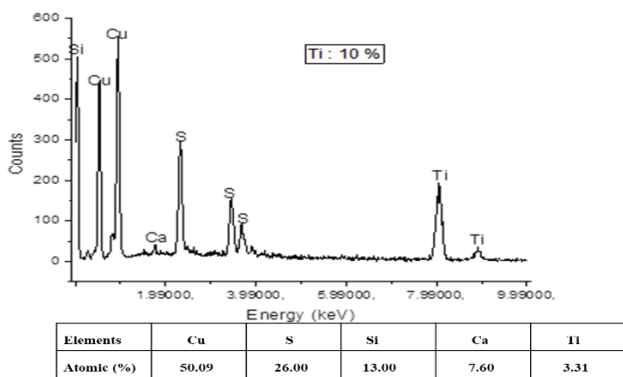


Figure 4.13 (b): EDS graph of Ti-doped CuS thin film

Table 4.4: Electrical properties of titanium-doped copper (II) sulfide thin films deposited at different titanium doping concentrations

Dopant Conc.	$V \times 10^{-3}$ (volts)	$I \times 10^{-5}$ (amps)	Thickness (nm)	$\rho \times 10^{-5}$ (Ωm)	$\sigma_e \times 10^3$ (S/m)
CuS	38.33	3.22	109.16	58.89	1.70
Ti: 2 %	3.77	1.70	113.17	11.37	8.70
Ti: 6 %	7.26	5.19	121.11	7.68	13.02
Ti: 10 %	10.18	6.51	131.79	9.34	10.71

4.7 Magnetic analyses of the deposited thin films

The magnetic properties of Ti-doped copper (II) sulfide thin films were analyzed using a vibrating sample magnetometer (VSM) at room temperature to study the impact of Ti ion substitution within a range of -60000 to 60000 (Oe). The findings are shown in Fig. 4.15. The magnetic hysteresis loops of the samples did not saturate, even when exposed to the highest measured field, showing their antiferromagnetic properties. Increasing Ti doping from 2% to 6% resulted in an increase in magnetization (M_{max}) from -0.00057 to 0.00048 emu/g – this is in agreement with (44). The increase in magnetization intensity of these films could be because of the changes in cation and anion valence during annealing and transformation of the crystalline structure caused by Ti doping. The highest magnetization rose as the titanium ion content increased. Also, the films showed low coercivity (H_c), and the results showed that higher permeability was associated with lower coercivity.

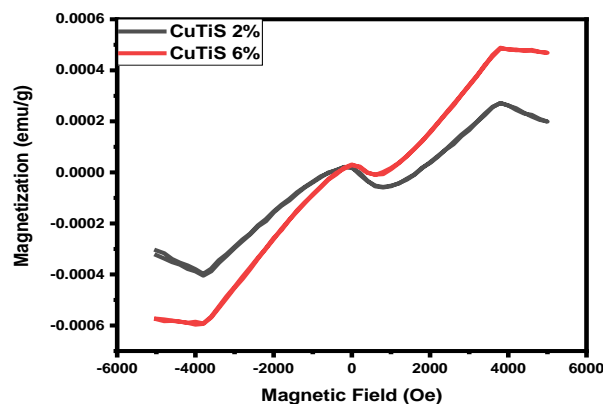


Figure 4.15: M – H Curves for Ti-doped CuS films deposited at 2 % and 6 % Ti conc.

From the energy bandgap, we could deduce that increase in percentage doping could increase the bandgap. This confirms replacement of other atoms by titanium.

From the M – H curve, the film deposited at higher percentage doping has higher magnetization, so increase in percentage

doping increases magnetization. This is in agreement with the work reported by (44).

There is a shift in the absorption spectrum observed in the optical result – this may be due to quantum confinement effects. The crystallites size of the films increased with increase in doping percentage – it may be attributed to the increase in the film thickness.

Electrodeposited Ti-doped CuS thin films show a thickness increase directly proportional to the Ti doping level. Similar trends in Zn-doped CuS films produced by chemical bath deposition were reported by Choudhury et al. (2020) [51], who attributed the increased film thickness to improved nucleation from dopant addition. According to Sankapal et al. (2005) [52], increasing dopants like In and Sn linearly increase the thickness of CuS films. Our results support previous research showing that dopants increase deposition rate and grain growth. Electrodeposited Ti-doped CuS thin films showed increased absorbance and decreased transmittance with Ti doping; bandgap energy ranged from 2.40–2.60 eV. In Ni-doped CuS films, Kumar et al. (2016)[53] found higher absorbance and lower transmittance. The reported band gap of undoped CuS is 2.2–2.5 eV [54], which aligns with the Burstein-Moss effect observed in doped semiconductors, explaining our observed band gap widening with Ti doping. Doping-induced carrier concentration changes in Al-doped CuS led to a bandgap widening from 2.25 to 2.55 eV [55]. Our optical findings align with past research on doped CuS films, suggesting that doping alters the band structure and enhances light absorption.

The hexagonal crystal structure of electrodeposited Ti-doped CuS thin films shows preferred (103) orientation. Crystallite size grew from approximately 27.8 nm to approximately 31.5 nm. With doping, dislocation density and strain lessened. Low-temperature deposition frequently produces hexagonal CuS with a (103) preferred orientation, according to Mane & Lokhande (2000)[56]. Increases in crystallite size and decreases in strain, similar to those observed in Ti- or Zn-doped semiconductors, were also reported in Ti-doped ZnO by Kumar et al. (2019)[57]. The observed structural changes, mainly larger crystallites and fewer defects, are characteristic of doped thin-film growth. Clustered particles; Parreira et al. (2012)[58] reported similar morphological improvements with optimal dopant levels in Cu-based sulfides. Our study also showed that over- or under-doping often results in uneven morphology or clumping. The SEM results support the established trend of improved film quality at moderate dopant concentrations. Increased resistivity and decreased conductivity resulted from doping. This behavior might appear illogical, since doping usually enhances conductivity. Despite its advantages, Ti, being a multivalent dopant, might introduce deep trap states or cause grain boundary scattering. Abdullah et al. (2018)[59] found that Ti doping in CdS reduced conductivity by increasing recombination centers. Our findings are credible and consistent with existing research on dopant-induced charge carrier scattering or defect states.

Antiferromagnetic behavior was observed in Ti-doped CuS thin films deposited through electrodeposition. CuS, without doping, usually shows no magnetism or only weak

diamagnetism. Introducing transition metal dopants (Ti) leads to antiferromagnetism or weak ferromagnetism. The findings on Ti-doped oxide semiconductors show similar unsaturated hysteresis loops[60]. The room-temperature antiferromagnetic signature is similar to other transition metal-doped systems. Our findings are consistent with the literature on doped CuS and similar chalcogenide thin films. The structural, optical, electrical, and magnetic properties are impacted by the dopant (Ti) as predicted. The antiferromagnetic behavior and higher electrical resistivity offer unique perspectives, especially considering the under-reported Ti doping in CuS in contrast to Zn, Ni, and Al doping.

CONCLUSION

With the use of electrodeposition technique, copper (II) sulfide thin film and Ti-doped copper (II) sulfide thin films have been successfully deposited onto conducting glass substrate (FTO), at room temperature. Thickness of the films were obtained using a profilometer, and the values obtained revealed that the films' thickness increased with increase in Ti doping concentration. Optical, structural, morphological, elemental, electrical, and magnetic properties of the electrodeposited films have been investigated, and observation showed that properties of the films were affected by the doping percentage. Optical absorbance values of the films were found to have increased as percentage of titanium was increased, while transmittance values of the films were found to have decreased as the dopant concentration was increased. Also, from the results obtained, Ti-doped CuS films recorded low reflection compared to the undoped CuS films. This could be attributed to the high absorbance nature of the films, caused by the thickness, which increased as the titanium percentage concentration was increased. Other optical properties such as extinction coefficient, refractive index, optical conductivity real and imaginary dielectric constants, and energy band gap were estimated using established expressions from our reviewed literatures. The energy bandgap varied from 2.40 eV to 2.60 eV, as the doping concentration was varied. EDS spectra of the films revealed atomic percentages of elements present in the films. The films crystallize well in the hexagonal structure with preferential orientation of the crystallites along the (103) plane. The average crystal sizes range from 27.761nm to 31.455 nm. The results obtained showed that, with the increase in dopant percentage, crystallite size of the films increased, while dislocation density and micro-strain decreased. The SEM images revealed agglomerated particles of different sizes and shapes. However, the film deposited at 6 % Ti doping has a better and homogeneous surface. Electrical conductivity and resistivity of the films varied with respect to the percentage doping. As conductivity decreased, resistivity increased. From the VSM analyses, the films exhibited clear hysteresis loops at room temperature, and there was no observed magnetic saturation, even at higher applied magnetic fields, which confirmed the antiferromagnetic nature of these films.

ACKNOWLEDGMENTS

The authors' profound gratitude goes to the Nigerian government for the provision of financial assistance in carrying

out this study, through Tertiary Education Trust Fund (TETFUND), with the reference number TETF/DR&D-CE/NRF 2021/SETI/ICT/00034/01. The authors are also grateful to Nano Research Forum of Nnamdi Azikiwe University, Awka, under the leadership of Prof. A. J. Ekpunobi, for all the support received.

CREDIT AUTHORSHIP CONTRIBUTION STATEMENT

All authors contributed to the study conception and methodology. Visualization and writing, Emmanuel O. Okechukwu. Original draft of manuscript, review, and editing were performed by Emmanuel O. Okechukwu, Azubuike J. Ekpunobi, Diemiruaye M. Jeroh, and Adline Nwodo. Data collection, analysis, and plotting of graphs were performed by Emmanuel O. Okechukwu, Nonso L. Okoli, Chidozie E. Okafor, and Overcomer Anusiuba. Supervision and Editing performed by Azubuike J. Ekpunobi. All authors have read and approved the final manuscript.

Conflicts of Interest: The authors declare no conflicts of interest.

Ethical Statement: The authors' research and findings are presented in full and precise detail in the article.

Data Availability Statement: The data that support the findings of this study are available upon request from the corresponding author.

REFERENCES AND NOTES

1. T. Neumann, S. Feldmann, P. Moser, et al. Manganese doping for enhanced magnetic brightening and circular polarization control of dark excitons in paramagnetic layered hybrid metal-halide perovskites. *Nat. Commun.* **2021**, 12 (1), 1–8.
2. A. Gupta, R. Zhang, P. Kumar, V. Kumar, A. Kumar. Nano-structured dilute magnetic semiconductors for efficient spintronics at room temperature. *Magnetochemistry* **2020**, 6 (1), 1–22.
3. S. Nemšák, M. Gehlmann, C.T. Kuo, et al. Element- and momentum-resolved electronic structure of the dilute magnetic semiconductor manganese doped gallium arsenide. *Nat. Commun.* **2018**, 9 (1), 1–8.
4. T. Dietl. A ten-year perspective on dilute magnetic semiconductors and oxides. *Nat. Mater.* **2010**, 9 (12), 965–974.
5. Z.H. Zhang, X. Wang, J.B. Xu, et al. Evidence of intrinsic ferromagnetism in individual dilute magnetic semiconducting nanostructures. *Nat. Nanotechnol.* **2009**, 4 (8), 523–527.
6. Y.Z. Jiao, D. V. Louzguine-Luzgin, K.F. Yao, Z.J. Zhang, N. Chen. A room-temperature magnetic semiconductor from a Co-Fe-Nb-B metallic glass. *Sci. China Physics, Mech. Astron.* **2023**, 66 (4), 1–6.
7. S.A. Wolf, D.D. Awschalom, R.A. Buhrman, et al. Spintronics: A spin-based electronics vision for the future. *Science (80-.)*. **2001**, 294 (5546), 1488–1495.
8. H.S. Kaushik. Dilute Magnetic Semiconductor: A Review of Theoretical Status. *Int. J. IT, Eng. Appl. Sci. Res.* **2014**, 3 (1), 2319–4413.
9. G. Murtaza, R. Ahmad, M.S. Rashid, et al. Structural and magnetic studies on Zr doped ZnO diluted magnetic semiconductor. *Curr. Appl. Phys.* **2014**, 14 (2), 176–181.
10. J. Philip, A. Punnoose, B.I. Kim, et al. Carrier-controlled ferromagnetism in transparent oxide semiconductors. *Nat. Mater.* **2006**, 5 (4), 298–304.
11. T. Mahalingam, C. Sanjeeviraja. Characterization of Electrodeposited Zinc Sulphide Thin Films. *Phys. Status Solidi* **1992**, 129 (2), K89–K92.
12. K.A. Mohammed, S.M. Ahmed, R.Y. Mohammed. Investigation of structure, optical, and electrical properties of cus thin films by cbd technique. *Crystals* **2020**, 10 (8), 1–22.
13. R.S. Ali, N.A.H. Al Aaraji, E.H. Hadi, et al. Effect of Lithium on Structural and Optical Properties of Nanostructured CuS Thin Films. *J. Nanostructures* **2020**, 10 (4), 810–816.
14. S.U. Offiah, F.I. Ezema, R.U. Osuji, S.C. Ezugwu. Structural and spectral analysis of chemical bath deposited copper sulfide thin films for solar energy conversions. *Dig. J. Nanomater. Biostructures* **2012**, 7 (1), 165–173.
15. P. V. Nho, P.H. Ngan, N.Q. Tien, H.D. Viet. Preparation and characterization of low resistivity CuS films using spray pyrolysis. *Chalcogenide Lett.* **2012**, 9 (10), 397–402.
16. J. Podder, R. Kobayashi, M. Ichimura. Photochemical deposition of Cu₂S thin films from aqueous solutions. *Thin Solid Films* **2005**, 472 (1–2), 71–75.
17. N.P. Huse, A.S. Dive, K.P. Gattu, R. Sharma. An experimental and theoretical study on soft chemically grown CuS thin film for photosensor application. *Mater. Sci. Semicond. Process.* **2017**, 67, 62–68.
18. N.A. Bakr, A.A. Kamil, M.S. Jabbar, H. Zeki. Deposition OF CuS , ZnS and their stacked layers thin films by chemical spray pyrolysis technique. *Sci.Int.(Lahore)* **2018**, 30 (2), 259–266.
19. N. Castillo, D. Olgún, A. Conde-Gallardo, S. Jiménez-Sandoval. Structural and morphological properties of TiO₂ thin films prepared by spray pyrolysis. *Rev. Mex. Fis.* **2004**, 50 (4), 382–387.
20. A.B.F. Martinson, J.W. Elam, M.J. Pellin. Atomic layer deposition of Cu₂S for future application in photovoltaics. *Appl. Phys. Lett.* **2009**, 94 (12), 123107.
21. C. Wu, J. Bin Shi, C.J. Chen, et al. Synthesis and optical properties of CuS nanowires fabricated by electrodeposition with anodic alumina membrane. *Mater. Lett.* **2008**, 62 (6–7), 1074–1077.
22. I. Saadon Najm, S. Mahmood Kadhim, A. Abdulkhaleq Alwahib. Investigation the CuS thin film prepared by pulsed laser deposition. *Mater. Today Proc.* **2021**, 42, 2609–2615.
23. S. Guangwei, M. Lixuan, S. Wensheng. Electrodeposition of one-dimensional nanostructures. *Recent Patents Nanotechnology* 3 (3), 182 – 191.
24. S. Thanikaikarasan, T. Mahalingam. Influence of solution pH in electrodeposited iron diselenide thin films. *J. Alloys Compd.* **2012**, 511 (1), 115–122.
25. A.K. Yıldırım, B. Altıokka. An investigation of effects of bath temperature on cdo films prepared by electrodeposition. *Applied Nanoscience (Switzerland)*. 2017, pp 513–518.
26. I.M. Dharmadasa, M.L. Madugu, O.I. Olusola, et al. Electroplating of CdTe thin films from cadmium sulphate precursor and comparison of layers grown by 3-electrode and 2-electrode systems. *Coatings* **2017**, 7 (2), 1 – 17.
27. J. Song, S.S. Li, S. Yoon, et al. Growth and characterization of CdZnS thin film buffer layers by chemical bath deposition. In *Conference Record of the IEEE Photovoltaic Specialists Conference; 2005*; pp 449–452.
28. D.M. Jeroh, A.J. Ekpunobi, D.N. Okoli. The Optical Properties of Europium-doped Zinc Selenide Films. *J. Nano- Electron. Phys.* **2020**, 12 (5), 1–5.
29. N.L. Okoli, L.N. Ezenwaka, N.A. Okereke, I.A. Ezenwa, N.A. Nwori. Investigation of Optical, Structural, Morphological and Electrical Properties of Electrodeposited Cobalt Doped Copper Selenide (Cu_{1-x}CoxSe) Thin Films. *Trends Sci.* **2022**, 19 (16), 5686.
30. S. Mahanty, D. Basak, F. Rueda, M. Leon. Optical properties of chemical bath deposited CdS thin films. *J. Electron. Mater.* **1999**, 28 (5), 559–562.
31. R. Ayinla, B.Y. Iyanda. Effect of Annealing on Solid State Properties of Zinc Oxide (ZnO) Thin Film Grown by Chemical Bath Deposition Method. *Int. J. Sci. Res. Phys. Appl. Sci.* **2023**, 8 (3), 60 – 64.
32. S. Sagadevan, I. Das. Chemical bath deposition (CBD) of zinc selenide (ZnSe) thin films and characterisation. *Aust. J. Mech. Eng.* **2017**, 15 (3), 222–227.
33. R. Bekkari, B. Jaber, H. Labrim, et al. Effect of solvents and stabilizer molar ratio on the growth orientation of sol-gel-derived ZnO thin films. *Int. J. Photoenergy* **2019**, 2019 (1), 1 – 7.

34. O.N. Ogada. Effect of Concentration of Reactants and Deposition Temperature on the Optical Properties of Iron-Doped Cadmium Stannate Thin Films Deposited on Glass Substrates By Spray Pyrolysis. *Am. J. Mater. Sci.* **2019**, 9 (1), 1–7.
35. A. Axelevitch, B. Gorenstein, G. Golan. Investigation of Optical Transmission in Thin Metal Films. *Phys. Procedia* **2012**, 32, 1–13.
36. S. Mushtaq, B. Ismail, M. Raheel, A. Zeb. Nickel Antimony Sulphide Thin Films for Solar Cell Application: Study of Optical Constants. *Nat. Sci.* **2016**, 08 (02), 33–40.
37. İ.A. Kariper. The production of UV absorber amorphous cerium sulfide thin film. *Mater. Res.* **2017**, 20 (5), 1345–1349.
38. E. Güneri. The Role of Au Doping on the Structural and Optical Properties of Cu₂O Films. *J. Nano Res.* **2019**, 58, 49–67.
39. P. Sharma, S.C. Katyal. Determination of optical parameters of a-(As₂Se₃)₉₀Ge₁₀ thin film. *J. Phys. D. Appl. Phys.* **2007**, 40 (7), 2115–2120.
40. N. Ifeyinwa Akpu, C. Adanma Sylvanus, E. Chinyere Nwaokorongwu, et al. Modulation of the physical properties of spray-deposited cobalt selenide nanofilm via yttrium doping for photovoltaic purposes. *J. Mater. Environ. Sci.* **2023**, 2023 (11), 1230–1244.
41. R. Mariappan, V. Ponnuswamy, P. Suresh. Effect of doping concentration on the structural and optical properties of pure and tin doped zinc oxide thin films by nebulizer spray pyrolysis (NSP) technique. *Superlattices Microstruct.* **2012**, 52 (3), 500–513.
42. H.M.M.N. Hennayaka, H.S. Lee. Structural and optical properties of ZnS thin film grown by pulsed electrodeposition. *Thin Solid Films.* 2013, pp 86–90.
43. A. Jafari-Rad, H. Kafashan. Preparation and characterization of electrochemically deposited nanostructured Ti-doped ZnS thin films. *Ceram. Int.* **2019**, 45 (17), 21413–21422.
44. L.K. Sharma, M. Kar, R.K. Choubey, S. Mukherjee. Low field magnetic interactions in the transition metals doped CuS quantum dots. *Chem. Phys. Lett.* **2021**, 780, 138902.
45. E. Güneri, A. Kariper. Optical properties of amorphous CuS thin films deposited chemically at different pH values. *J. Alloys Compd.* **2012**, 516, 20–26.
46. E.O. Ojegu, B.U. Osolobri, E.I. Onyesom, et al. Yttrium incorporation into the tungsten telluride (Y:WTe₂) matrix achieved using three electrode systems. *Mater. Nanosci.* **2025**, 12 (1), 1185.
47. A. Jafari-Rad, H. Kafashan. Preparation and characterization of electrochemically deposited nanostructured Ti-doped ZnS thin films. *Ceram. Int.* **2019**, 45 (17), 21413–21422.
48. E.O. Okechukwu, D.N. Okoli. Optical And Structural Properties of Electrodeposited CdS / ZnS Compound Thin Films and Their Possible Applications. *J. Mater. Sci. Appl.* **2015**, 1 (6), 282–291.
49. F.M. Tezel, İ.A. Kariper. Effect of pH on optic and structural characterization of chemical deposited AgI thin films. *Mater. Res.* **2017**, 20 (6), 1563–1570.
50. C. Awada, G.M. Whyte, P.O. Offor, et al. Synthesis and studies of electro-deposited yttrium arsenic selenide nanofilms for opto-electronic applications. *Nanomaterials* **2020**, 10 (8), 1–15.
51. K.H. Rahman, A.K. Kar. Titanium-di-oxide (TiO₂) concentration-dependent optical and morphological properties of PANi-TiO₂ nanocomposite. *Mater. Sci. Semicond. Process.* **2020**, 105, 104745.
52. M. Mracek, J. Wallaschek. A system for powder transport based on piezoelectrically excited ultrasonic progressive waves. *Mater. Chem. Phys.* **2005**, 90 (2–3), 378–380.
53. R.X. Silva, A.S. De Menezes, R.M. Almeida, et al. Structural order, magnetic and intrinsic dielectric properties of magnetoelectric La₂CoMnO₆. *J. Alloys Compd.* **2016**, 661, 541–552.
54. S. Inoue, K. Ueda, H. Hosono, N. Hamada. Electronic structure of the transparent p-type semiconductor (LaO)CuS. *Phys. Rev. B* **2001**, 64 (24), 245211.
55. E. Güneri, A. Kariper. Optical properties of amorphous CuS thin films deposited chemically at different pH values. *J. Alloys Compd.* **2012**, 516, 20–26.
56. R.S. Mane, C.D. Lokhande. Chemical deposition method for metal chalcogenide thin films. *Mater. Chem. Phys.* **2000**, 65 (1), 1–31.
57. R. Ade, S.S. Kumar, S. Valanarasu, et al. Enhanced optoelectronic properties of Ti-doped ZnO nanorods for photodetector applications. *Ceram. Int.* **2021**, 47 (17), 24031–24038.
58. N.D. Scarisoreanu, A. Andrei, R. Birjega, et al. Electrical and optical investigations on Pb_{1-3x/2}La_xZr_{0.2}Ti_{0.8}O₃ thin films obtained by radiofrequency assisted pulsed laser deposition. *Thin Solid Films* **2012**, 520 (14), 4568–4571.
59. K. Binidra, R. Miloua, M. Khadraoui, et al. Spectral control in thermophotovoltaic systems by optimized one-dimensional photonic crystals. *Optik (Stuttg.)* **2018**, 156, 879–885.
60. R. Rakhshae, Y. Noorani. Comparing three methods of simultaneous synthesis and stabilization of Fe₃O₄ nanoparticles: Changing physicochemical properties of products to improve kinetic and thermodynamic of dye adsorption. *J. Magn. Magn. Mater.* **2017**, 422, 128–140.

AUTHORS BIOGRAPHIES

Emmanuel O. Okechukwu: <https://orcid.org/0009-0007-8316-3356>